

Resonant nonstationary amplification of polychromatic laser pulses and conical emission in an optically dense ensemble of neon metastable atoms

S. N. Bagayev,¹ V. S. Egorov,² I. B. Mekhov,² P. V. Moroshkin,² I. A. Chekhonin,² E. M. Davliatchine,³ and E. Kindel³

¹*Institute of Laser Physics, Siberian Branch of the Russian Academy of Sciences, Lavrentyeva 13/3, 630090 Novosibirsk, Russia*

²*St. Petersburg State University, Department of Optics,
Uljanovskaya 1, Petrodvorets, 198504 St. Petersburg, Russia*

³*Institut für Niedertemperatur-Plasmaphysik, Friedrich-Ludwig-Jahn-Str. 19, 17489 Greifswald, Germany*

(Dated: April 3, 2003)

Experimental and numerical investigation of single-beam and pump-probe interaction with a resonantly absorbing dense extended medium under strong and weak field-matter coupling is presented. Significant probe beam amplification and conical emission were observed. Under relatively weak pumping and high medium density, when the condition of strong coupling between field and resonant matter is fulfilled, the probe amplification spectrum has a form of spectral doublet. Stronger pumping leads to the appearance of a single peak of the probe beam amplification at the transition frequency. The greater probe intensity results in an asymmetrical transmission spectrum with amplification at the blue wing of the absorption line and attenuation at the red one. Under high medium density, a broad band of amplification appears. Theoretical model is based on the solution of the Maxwell-Bloch equations for a two-level system. Different types of probe transmission spectra obtained are attributed to complex dynamics of a coherent medium response to broadband polychromatic radiation of a multimode dye laser.

PACS numbers: 42.50.Gy, 42.50.Md, 42.50.Fx, 42.65.-k

I. INTRODUCTION

We present a systematical experimental study of resonant interaction between broadband pulsed-laser radiation and an optically dense extended two-level medium. In our experiments, the pump-probe configuration was used and probe beam amplification and/or attenuation were studied in detail. Single pump beam propagation was investigated as well, and some off-axis radiation, which is usually referred to as conical emission, was observed. A theoretical model is based on the solution of the semiclassical Maxwell-Bloch equations taking into account propagation effects of the electromagnetic field.

Investigation of resonant interactions in optically dense media is of particular interest. In the case where the density of resonant particles is high enough that a sufficient part of the external field can be coherently absorbed and reemitted by the medium, a strongly coupled system of photons and medium excitations, polaritons, is effectively created, and collective phenomena play a key role in the interaction processes [1]. Some specific amplitude and phase (dispersive) characteristics that arise under this regime lead to the appearance of coherent phenomena, which significantly affect and enlarge the interaction picture. Particularly, many-atom vacuum Rabi oscillations [2, 3] and optical ringing [4] reflect the coherent beating of two normal modes of the coupled field-matter systems, which can be described as a splitting of polariton dispersion curve into two branches. Such nonlinear effects as polariton parametric amplification in semiconductor microcavities [5, 6, 7] and a phenomenon of spectrum condensation in atomic and molecular media [8, 9] were observed in intracavity experiments under the large vacuum Rabi splitting.

The pump-probe experiments with gaseous resonantly absorbing media have been reported in numerous publications. When the pump beam carrier frequency ω_{pump} is fixed and the probe beam frequency ω_{probe} is scanned near the frequency of an atomic transition ω_0 , the probe-beam transmission has a form of the well-known Mollow-Boyd spectrum [10, 11, 12]. Its spectral features are determined by a value of the generalized Rabi frequency of the strong field applied. Although the theory [10, 11, 12] is developed for the steady-state regime, it describes the pulsed-laser experiments [13, 14] as well as experiments with cw lasers [15]. Recently, the steady-state theory was generalized for nonstationary processes using numerical solution of the Maxwell-Bloch equations [16]. In all of these experiments, the generalized Rabi frequency of the pump beam is much greater than the spectral widths of the atomic transition, γ_2 , and both laser pulses γ_{pump} and γ_{probe} . Besides that, a medium coherently absorbs and reemits a small portion of the laser pulse energy, hence the field of the medium response can be neglected with respect to the strong external field. In this case, the theory of light-matter interaction is reduced to the consideration of a single atom driven by the strong electromagnetic field.

Conical emission (CE) in gaseous atomic media was discovered by Grischkowsky in 1970 [17] and investigated in detail by many researchers. A comprehensive review can be found in Ref. [18]. CE is usually observed when intense laser radiation (cw or pulsed), detuned to the blue side from an atomic resonance, propagates in a dense resonant medium. The spectrum of CE is usually much broader than γ_{pump} and shifted to the red side of an absorption line. Despite all efforts, only CE under cw pumping has received a complete theoretical explanation.

tion [19]. Moreover, several different types of CE were observed in some experiments [20, 21], suggesting that several possible mechanisms of CE generation exist. Influence of collective effects on the conical emission was discussed in Refs. [14, 22].

In cw experiments, spectral width of the laser radiation is usually much less than both homogeneous γ_2 and inhomogeneous (Doppler) γ_D widths of an atomic transition. In all pulsed experiments discussed above, laser radiation has a form of smooth bell-shaped pulses with spectral width, determined by the pulse duration such that $\gamma_{\text{pump}}, \gamma_{\text{probe}} > \gamma_2$ and $\gamma_{\text{pump}}, \gamma_{\text{probe}}$ are of the same order of magnitude as γ_D . In the present work, we consider quite a different situation: the spectral width of laser pulses is determined by the number of longitudinal modes (more than 100) of a multimode dye laser and is much greater than the inverse pulse duration and both γ_2 and γ_D . This enables us to study interaction of radiation with both red and blue polariton branches simultaneously. The envelope of such a broadband polychromatic pulse consists of a great number of very short irregular peaks. Detunings of the pump and probe pulses from the transition frequency, defined as $\Delta_0 = \omega_{\text{pump}} - \omega_0$, $\delta_0 = \omega_{\text{probe}} - \omega_0$, are much smaller than the spectral widths of both lasers, γ_{pump} and γ_{probe} (here ω_{pump} and ω_{probe} correspond to mean frequencies of the pump and probe spectra). The pump beam intensity J_{pump} was scanned in the range that corresponds to the Rabi frequency $\Omega < \gamma_{\text{pump}}$. The relation between values of γ_{pump} , γ_D , and Ω considered in the present paper characterizes a system, which up to now was not investigated systematically. Resonant interaction of atomic media and broadband pulses was considered only in some works on self-induced transparency (SIT) in the sharp line limit [23, 24] (see also Ref. [38]) and in intracavity experiments, where the phenomenon of self-frequency-locking, or spectrum condensation, was studied [8, 9].

The paper is organized as follows. In Sec. II, our experimental setup is described. In Sec. III, the experimental results are presented, being divided into three parts: probe-beam transmission under extremely broadband pump, probe-beam transmission under relatively narrow-band pump, and conical emission measurements. Section IV is devoted to the theoretical model, numerical simulation, and discussion of the experimental data. Main results are summarized in Sec. V.

II. EXPERIMENTAL SETUP

The scheme of our experimental setup is presented in Fig. 1. We used two pulsed multimode dye lasers (1, 2) pumped by the same Nd:YAG (where YAG stands for yttrium aluminium garnet) laser (3) for the pump-probe experiments. The pulse duration of both dye lasers was about 7 ns, the probe-beam spectral width was about 1 nm. The dye laser (1) producing the pump beam has two operation modes with different spectral widths: “broad-

band” mode $\gamma_{\text{pump}}/2\pi \approx 300$ GHz (with a prism inside the cavity) and “narrowband” mode $\gamma_{\text{pump}}/2\pi \approx 10$ GHz (with a diffraction grating inside the cavity). The pump beam intensity J_{pump} was scanned in a range of $10^4 - 10^6$ W/cm² (measured pulse energies 1-100 μ J) by rotation of a polarizer P2. The pump and probe beams were intersected at the angle of about 1° inside a discharge tube (4) containing a resonant medium. The probe beam spectrum was analyzed by means of a high-resolution spectrograph constructed on the optical table. The spectral resolution was about 12 GHz. The spectra were recorded by a charge-coupled device (CCD) camera (8) with 100 ns exposure time. Because of great fluctuations of the multimode dye-laser intensity, we averaged recorded probe beam spectrum over 500 pulses. To control wavelength tuning of the dye laser (1), part of its radiation was directed to the same high-resolution spectrograph by a beam splitter (5) and a system of mirrors.

The wavelengths of both dye lasers were tuned to a transition of neon $1s_5 - 2p_9$ in Paschen notation ($\lambda=640.2$ nm) with a metastable lower state. This is the strongest red line of neon spectrum. A pulsed neon discharge was used to produce sufficient amount of metastable neon atoms. The discharge tube has a diameter of 10 mm and the length $L = 12$ cm. The amplitude of the discharge current was $I = 4.0 - 4.5$ A, pulse duration $t_p = 80 - 100$ μ s, neon pressure $P = 9 - 14$ Torr. Under these conditions in the discharge afterglow, the metastable atom density n_0 reaches great values up to 10^{13} cm⁻³. The optical density was scanned in a range of $\alpha_0 L \approx 20 - 200$ by changing the time delay τ_d between the discharge current and the laser pulse. Here α_0 is the absorption coefficient at the center of Doppler-broadened absorption line. Experiment was also performed with a dc discharge in neon in the same discharge tube under the conditions of $I = 2 - 50$ mA and $P = 0.5 - 3.5$ Torr. In a dc discharge, metastable atom density was about 10^{12} cm⁻³. We controlled this value by measuring the resonant absorption across the discharge tube. A well-known technique with a mirror behind the discharge tube was used (mirror M9 in Fig. 1). In this configuration the same discharge tube serves as an absorber and a light source. A spectrograph (10) with a CCD camera (11) was used for these measurements.

III. EXPERIMENTAL RESULTS

A. Pump-probe experiment with broadband pump

The results of our pump-probe experiments with broadband pump beam are presented in Figs. 2 - 7. In Fig. 2(a), typical spectra of the pump beam with discharge switched off (curve A) and on (curve B) are plotted. The absorption line contour is partially resolved and shows the position of the atomic resonance. Here the pump pulse energy W is about 30 μ J. At greater power there is no absorption because of the medium sat-

uration. Figure 2(b) shows the probe beam spectra under the same conditions with pump beam switched on (the pump pulse energy $W \approx 80 \mu\text{J}$).

We observed significant (up to six times) amplification of some spectral components of the probe beam. In Figs. 3 - 6, the most characteristic probe transmission spectra $K(\delta)$ are presented, where $K(\delta) = J(\delta)/J^0(\delta)$, $\delta = \omega - \omega_0$ is the detuning from the atomic resonance, $J(\delta)$ is the probe beam spectrum after its interaction with the medium, and $J^0(\delta)$ is the original probe beam spectrum. Systematical investigation of these spectra has shown that there exist four amplification modes with different characteristic shapes of the amplification spectrum: (i) spectrum with a single peak at the resonance frequency (curve A in Fig. 3); (ii) doublet centered at the resonance frequency with partially saturated absorption line (curve C in Fig. 3, Fig. 4); (iii) spectrum of dispersionlike shape (Fig. 5); and (iv) spectrum with a resonant peak and a broad ‘‘pedestal’’ (Fig. 6). Four separate series of measurements are presented below to clarify how the shape of the spectrum depends on the main parameters of our experiment: J_{pump} , J_{probe} , n_0 , and Δ_0 . The latter dependence was performed under the narrowband pumping and is presented in Sec. III B.

1. Scanning of the pump intensity

Transmission spectra of the probe beam at different pump powers under fixed J_{probe} are presented in Fig. 3. Curve A in Fig. 3 corresponds to the pair of spectra in Fig. 2(b) and represents amplification spectrum of the first type, with a single resonant peak. It appeared under significant pump beam intensities ($W > 30 \mu\text{J}$). The dependence of the transmission at the resonance frequency K_0 on the pump pulse energy W is shown in Fig. 7.

Decrease in the pump beam power below $W = 30 \mu\text{J}$ leads to the splitting of this peak into a doublet, i.e., spectrum of the second type, as it is shown by curves B and C in Fig. 3. Spectra of the second type were investigated in detail by means of a scanning Fabry-Perot interferometer with 500 MHz spectral resolution (cf. Refs. [25, 26]). For this experiment both the pump and probe beams were obtained from the same dye laser with the spectral width $\gamma_{\text{pump}}/2\pi \approx 30 \text{ GHz}$. Different transition with the same metastable lower state was used ($\lambda=588.2 \text{ nm}$). One can find a more detailed description of the experimental setup and the results obtained in Refs. [25, 26]. Typical transmission spectra are presented in Fig. 4. As it is shown, the components of the doublet are symmetrically detuned from the resonance frequency. There is significant absorption near the resonance. Both components of the doublet decrease, with pump beam power decreasing and completely disappearing when light-matter interaction becomes linear.

2. Strong probe beam

Increase in the probe beam power results in transmission spectra of the third type (Fig. 5). Some asymmetry in transmission spectrum appears under greater probe beam power even without the pump beam. This is clearly seen in Fig. 5 (curve B), where the single probe beam transmission is shown. For the case of the weak probe beam, there is no such asymmetry, as one can see in Fig. 3 (curve D) and Fig. 4 (curve B). With the pump switched on, this asymmetry becomes much more pronounced. There is strong amplification in the blue wing of the absorption line and attenuation in the red wing. Antisymmetrical spectrum, shown by curve A in Fig. 5, was observed under moderate pumping ($W = 20 - 30 \mu\text{J}$). Decrease in the pump beam power under fixed probe power leads to the decrease in the amplification coefficient at blue detunings, while at higher pump intensities the amplification increases. In the latter case the probe-beam energy integrated over the whole spectrum is amplified, which evidenced the existence of energy transfer from the pump beam.

3. Increase of the optical density

Spectra of the first, second and third type were observed in a broad range of metastable atom densities n_0 : from $5 \times 10^{11} \text{ cm}^{-3}$ (in a dc discharge), up to 10^{13} cm^{-3} (in a pulsed discharge afterglow). Increase in the n_0 value leads to higher efficiency of the probe amplification in both the first and second amplification regimes. In the case of the strong probe beam (third regime), evolution of the transmission spectrum is more complicated. The increase in n_0 resulted in (i) broadening of the dispersionlike feature, (ii) increase in the absorption at the resonance frequency, and (iii) increase in the amplification at the wing of the absorption line.

Moreover, at maximum atomic density, another, fourth type of the amplification spectrum was observed (Fig. 6). In the pulsed discharge experiment, the metastable atom density rapidly increases in the afterglow, when the discharge current is switched off, reaches its maximum value (about 10^{13} cm^{-3}), and then slowly decreases (the time interval between the discharge pulses was much greater than the characteristic decay time of n_0). Curves A - C in Fig. 6 show how the spectrum of the fourth type varies with the time delay between the discharge and laser pulses. Amplification reaches its maximum at the delay of $80 \mu\text{s}$, when n_0 has a maximum. The transmission spectrum of this type is a superposition of the resonant peak, described above as the first-type spectrum, and the broadband amplification at the red side of the absorption line. The spectral width of this band is extremely large, up to 350 GHz.

B. Pump-probe experiment with narrowband pump

The dependence of the probe transmission spectrum on the pump detuning Δ_0 was studied under the “narrowband” pumping. For these measurements the dye laser (1), producing the pump beam, was switched to the narrowband mode (see Sec. II) with the spectral width [full width at half maximum (FWHM)] $\gamma_{\text{pump}}/2\pi = 10$ GHz. Here, Δ_0 corresponds to the detuning between the center of the pump spectrum and the atomic transition. Typical pump spectrum is shown by the curve C in Fig. 8. Comparison of this curve with Fig. 2(a) explains the difference between the broadband and narrowband mode.

An earlier version of our experiment was presented in Ref. [27]. Amplification spectra, observed in Ref. [27] under narrowband pumping, were similar to the first and third types described above. The main disadvantage of our earlier experiments [25, 26, 27] was that both the probe and pump beam were obtained from the same dye laser. Scanning the frequency of the laser in Ref. [27] revealed some interesting behavior of the amplification coefficient value, while the shape of the transmission spectrum was not affected. In the first amplification regime with the “resonant peak” spectrum, amplification is the most effective under resonant pumping $\Delta_0 = 0$, while in the third regime with the dispersionlike spectrum, amplification reaches its maximum, when the pump is detuned to the blue side from the resonance at $\Delta_0 = 7$ GHz. The present experimental setup allows us to scan the pump frequency keeping the probe spectrum fixed. The results of the present study are in general agreement with the data reported in Ref. [27]. Typical result of this experiment is presented in Fig. 8 demonstrating the dispersionlike amplification contour.

C. Conical emission

In the series of measurements with metastable atom density of about 10^{13} cm $^{-3}$ (in pulsed discharge afterglow) and great pump beam intensity ($W \approx 50 - 100$ μJ in a “broadband” mode, or about 10 μJ in a “narrowband” mode), we observed the amplification of radiation in the periphery of the pump beam, appeared independently on the probe-beam presence. This radiation propagates at the angle of $\theta = 10 - 15$ mrad with respect to the pump beam and forms a cone around it. In the literature, this phenomenon is usually referred to as conical emission. It should be emphasized that in this domain, all known experiments were carried out in vapors of alkali and rare-earth elements. Here we present the first conical emission observed in a noble gas.

The transverse profile of the radiation after its passage through the discharge tube was recorded by the same CCD camera that was used for the probe-beam spectrum investigation. For this experiment the camera was installed at a distance of 1 m behind the discharge tube.

The central and the most intense part of the pump beam was blocked to avoid damage of the camera. In Fig. 9, a typical image taken by the camera is shown. The inner ring in this picture corresponds to the periphery of the pump beam, whereas the outer one represents the conical emission. In a range of parameters explored, we did not find any dependence of the cone angle θ on J_{pump} or n_0 . Increase in the time delay τ_d leads to the decreasing medium density and cone intensity.

We also observed conical emission in the experiments with narrowband pump. In this regime, the cone intensity depends on the pump detuning Δ_0 : it has two maxima on the wings of the absorption line and disappears at the large detunings $|\Delta_0/2\pi| > 10$ GHz. This dependence is plotted in Fig. 10.

The conical emission spectra were recorded together with the probe-beam spectra under the same conditions. We observed spectra with shapes very similar to the probe-beam amplification spectra (except for the dispersionlike contour). One example of the conical emission spectrum under broadband pumping is shown in Fig. 11. The single peak is situated near the atomic resonance and is shifted to the red side. This fact is in agreement with other conical emission experiments, although the width of the peak and its detuning are different.

IV. THEORETICAL MODEL AND DISCUSSION

A. Equations of the model

Theoretical model is based on the solution of the semi-classical Maxwell-Bloch equations in the two-level approximation [28]. Using the rotating wave approximation, the system of Bloch equations can be written as

$$\frac{\partial p}{\partial t} = \Omega D - \gamma_2 p, \quad (1a)$$

$$\frac{\partial D}{\partial t} = -\frac{1}{2}(\Omega p^* + \Omega^* p) - \gamma_1 (D - D^{eq}), \quad (1b)$$

where $\Omega = 2dE/\hbar$ is the complex Rabi frequency of the electromagnetic field (d is the electric dipole moment of the atomic transition), p and D are the complex polarization and population difference of atoms, and D^{eq} is the value of D in the absence of external field (the value $D = 1$ corresponds to an atom in the ground state). The relaxation rates γ_1 and γ_2 determine the homogeneous broadening of a spectral line. Here Ω and p are the functions slowly varying in time but having arbitrary spatial dependence.

The problem of the interaction between two intersected plane linearly polarized waves was considered. In this case, the amplitude of the field is given by

$$\Omega = \Omega_0(t, z)e^{-ik_0z} + \Omega_1(t, z)e^{-ik_1r}, \quad (2)$$

with Ω_0 and Ω_1 slowly varying in space. The field Ω_0 with a wave vector \mathbf{k}_0 parallel to the z axis corresponds to the strong pump wave, whereas Ω_1 with \mathbf{k}_1 wave vector is assumed to be a weak probe field propagating at a small angle of φ with respect to z direction. Nonlinear interaction of the intersected waves leads to the appearance of spatial polarization harmonics with wave vectors $\mathbf{k}_0 + m\Delta\mathbf{k}$ ($m = 0, \pm 1, \pm 2, \dots$, $\Delta\mathbf{k} = \mathbf{k}_1 - \mathbf{k}_0$) and harmonics of the population difference with $m\Delta\mathbf{k}$ wave vectors:

$$p = \sum_{m=-\infty}^{\infty} p_m(t, z) e^{-i(\mathbf{k}_0\mathbf{r} + m\Delta\mathbf{k}\mathbf{r})}, \quad (3a)$$

$$D = \sum_{m=-\infty}^{\infty} D_m(t, z) e^{-im\Delta\mathbf{k}\mathbf{r}}, \quad D_m = D_{-m}^*. \quad (3b)$$

The emission of the p_0 and p_1 polarizations corresponds to the pump and probe fields, respectively. The emission of higher harmonics is considered to be suppressed in a thick medium, due to mismatch in dispersion relation, which is in agreement with our experimental conditions. Substituting expansions (2) and (3) into Eq. (1), and using the first-order perturbation theory in respect of the small amplitude of the probe field, one can get a system of the Maxwell-Bloch equations, describing propagation of the strong pump field,

$$c \frac{\partial \Omega_0}{\partial z} + \frac{\partial \Omega_0}{\partial t} = -\omega_c^2 p_0, \quad (4a)$$

$$\frac{\partial p_0}{\partial t} = \Omega_0 D_0 - \gamma_2 p_0, \quad (4b)$$

$$\frac{\partial D_0}{\partial t} = -\frac{1}{2} (\Omega_0 p_0^* + \Omega_0^* p_0) - \gamma_1 (D_0 - D^{eq}), \quad (4c)$$

and a weak probe,

$$c \cos \varphi \frac{\partial \Omega_1}{\partial z} + \frac{\partial \Omega_1}{\partial t} = -\omega_c^2 p_1, \quad (5a)$$

$$\frac{\partial p_1}{\partial t} = \Omega_1 D_0 + \Omega_0 D_1 - \gamma_2 p_1, \quad (5b)$$

$$\frac{\partial D_1}{\partial t} = -\frac{1}{2} (\Omega_1 p_0^* + \Omega_0^* p_1 + \Omega_0 p_{-1}^*) - \gamma_1 D_1, \quad (5c)$$

$$\frac{\partial p_{-1}^*}{\partial t} = \Omega_0^* D_1 - \gamma_2 p_{-1}^*, \quad (5d)$$

where

$$\omega_c = \sqrt{\frac{2\pi d^2 \omega_0 n_0}{\hbar}} \quad (6)$$

is the cooperative frequency of the medium, which plays a role of the coupling coefficient between field and matter, and n_0 is the density of atoms in the ground state.

The character of resonant coherent interaction between laser field and an ensemble of two-level atoms is determined by the atomic density and particular characteristics of laser pulse, such as the area and energy. Temporal features of propagating pulse strongly depend on

the condition whether the field reemitted by the medium is comparable to the field that has been externally applied. In the limiting case, where reemission field is negligible in comparison to the strong externally applied one, the model of single driven atom is usually used. Atomic response is calculated on the basis of Bloch equations, whereas Maxwell equations are not taken into account. Thus, the dynamics of the system is fully determined by the strong external field. In this context, phenomena such as Rabi sideband generation due to stationary probe-pump Mollow-Boyd effect [10, 11, 12] or to transient Rabi flopping [28] can be mentioned.

In a system, where the field of medium reaction plays an essential role, Bloch and Maxwell equations are considered self-consistently. In the case of a single (pump) field propagation, under the simplest conditions of an amplitude modulated signal, and in the limit of coherent interaction $\gamma_{1,2} = 0$, Eqs. (4) can be reduced to the nonlinear evolution sine-Gordon equation, which describes the coherent breakup of a laser pulse into solitons (2π pulses or breathers) [29] and a nonsolitonic solution in the form of the so-called optical ringing [30]. 2π solitons of self-induced transparency represent the pulses, where the coherently absorbed and reemitted fields are balanced. Nevertheless, in this case, the field applied is still strong enough to invert a part of a medium (area of the external field is greater than π).

In accordance with the area theorem [28], if the area of the input field takes the value less than π , the nonstationary dynamics of the pulse breakup into 2π solitons cannot be realized. On the other hand, in an optically dense coherent medium, another type of field oscillations, optical ringing, appears. This oscillating response has a superradiant character [4] and appears in the system of strongly coupled field and matter, where the high density of resonant atoms provides the atomic system to be able to coherently absorb and reradiate whole energy of the weak external electromagnetic field. The oscillations display the process of fast excitation interchanges between field and a two-level atomic ensemble in an extended resonant medium and the formation of a 0π pulse. Such cooperative interactions are the transient phenomena and can be observed when the frequency of the photon interchanges between field and matter greatly exceeds relaxation rates of a medium.

The collective oscillations can be treated as beating between two normal modes of coupled linear oscillators, which correspond to splitting of the polariton (coupled matter photons) dispersion curve into two branches. Thus, contrary to nonlinear strong-field effects, the coherent dynamics of strongly coupled field-matter system originates from linear (weak-field) dispersion, where field and polarization components are represented by equal contributions, and reemission field plays an essential role in the light-matter interaction. Vacuum Rabi oscillations (both single- and many-atom oscillations) [2, 3] are cavity analogs of such processes. In the simplest case of a single-mode cavity, the frequency of field and polariza-

tion oscillations is equal to the cooperative frequency of the medium, ω_c , when the condition of strong-coupling regime $\omega_c \gg \gamma_2$ is fulfilled. Under free-space interactions, the frequency of field-matter photon interchanges is also determined by the coupling coefficient (6). To observe coherent beating of two (red and blue) polariton branches, they should be excited by the laser field simultaneously. In our experiment, this condition is fulfilled due to resonant broadband (much broader than the Doppler linewidth) spectrum of the radiation used.

B. Numerical results

We studied numerically interaction of polychromatic broadband quasistochastic laser pulses in a dense medium without population inversion. The parameters of numerical simulations were similar to the experimental conditions. Input pump field was chosen to have the following form:

$$\begin{aligned} \Omega_0(t, 0) &= C(t) \sum_{k=-N}^{k=N} \Omega_{0k} e^{i(\Delta_0 t + \omega_k t + \alpha_k)}, \\ \Omega_{0k} &= \Omega_{00} e^{-4 \ln 2 (\omega_k / \gamma_{\text{pump}})^2}, \\ C(t) &= \frac{2}{\pi} e^{-(t-t_0)/a} \left[\frac{\pi}{2} + \arctan \left(\frac{t-t_0}{b} \right) \right], \end{aligned} \quad (7)$$

where $\omega_k = k\Delta\omega$ ($k = 0, \pm 1, \dots, \pm N$) are the modes of the input spectrum, $\Delta\omega$ is the intermode distance, Δ_0 is the detuning between the central frequency of the field and that of the atomic resonance, and α_k are the mode phases. The phases are random numbers, which leads to the quasistochastic temporal dependence of the electric field. The duration of this signal does not depend on the width of the spectrum γ_{pump} , but is determined by the duration of the envelope, $C(t)$.

Modeling one of the experimental realizations, we used the following parameters of the input signal: $\Delta\omega/2\pi = 0.37$ GHz, $\gamma_{\text{pump}}/2\pi = 20.0$ GHz (thus, the number of modes was about 100), the duration of the envelope, $C(t)$, was equal to 3.5 ns ($a = 2.4$ ns, $b = 0.3$ ns). The amplitude of the probe field has the form $\Omega_1(t, 0) = \Omega_0(t - \tau_0, 0)/g$, where $g \gg 1$, and a short (about 10 ps) time delay τ_0 between the fields was taken into account. The atomic transition with $\gamma_1/2\pi = 8.4$ MHz and $\gamma_2/2\pi = 5.4$ MHz was considered. The cooperative frequency of the medium was equal to $\omega_c/2\pi = 2.6$ GHz and the length of the medium $L = 15$ cm. Since correlation time of the field was much smaller than the pulse duration, and great number of modes were considered, main spectral features of the output field were not sensitive to the certain realization of random phases and a small time delay τ_0 existing in the experiment.

A typical example of the temporal behavior of the single (pump) field at the output of the extended medium is presented in Fig. 12. The figure shows that during

the propagation of the multimode radiation (7) through a resonant extended medium, smooth slow solitons separate from the quasistochastic part, that forms the initial stage of the signal. The optical ringing accompanies the creation of a soliton and forms the tail of the light pulse. If the area of the input pulse takes the value less than π , 2π solitons are not created and the optical ringing signal can be the only and dominant part at the pulse tail. Thus, Fig. 12 shows the transformation of the quasistochastic signal with correlation time determined by the width of the input spectrum, γ_{pump} (7), into the coherent response of the dense resonant medium, determined mainly by the field-matter coupling coefficient ω_c (6) and by the length of the medium, L .

The numerical study was based on the joint solution of Eqs. (4) and (5). In Fig. 13, spectra of the probe field at the input and output of the medium are displayed. The spectra presented were obtained by convoluting the calculated spectra with a smooth Gaussian function, modeling the transmission of the signal through a device with finite resolution, so single modes of the polychromatic signal are not resolved. Depending on the pump intensity, two types of the probe amplification were obtained.

If the pump field is strong enough to produce non-stationary population inversion in a two-level extended medium, the probe is significantly amplified at the resonance frequency [Fig. 13(b)]. The most essential growth of the probe field is obtained in the space and time areas, where a smooth 2π soliton has formed in the pump beam, which leads to the slow rotation of the Bloch vector and smooth variation of the population difference between 1 and -1 values, which corresponds to transitions of the atoms from the ground state to the excited one and back through the coherent superposition states.

In the case of relatively small pumping intensity, the pump pulse can propagate without producing a soliton. This condition leads to oscillations of the Bloch vector near the equilibrium point $D = 1$. Here, the amplification spectrum obtained corresponds to the spectral doublet presented in Fig. 13(a). Moreover, a slow soliton separated from the main fast part of the signal can be absorbed in the medium during the propagation. As a result, even in this case, amplification is formed by the fast part of the signal (quasistochastic and ringing), which has the area equal to zero, which, again, corresponds to the doublet in the amplification spectrum. As was shown in Refs. [25, 26] (see also Ref. [38]), under some conditions, the interaction of 0π pulses in a dense medium results in amplification of the coherent optical ringing. Besides that, two maxima in the amplification spectrum can be parametrically coupled due to the modulation of the population difference by the pump field.

The doublet and single-maximum characters of the probe amplification under the weak and strong pumping, respectively, qualitatively correspond to our experimental observations presented in Figs. 3 and 4. The origin of such spectral behavior of the probe field can be traced to the dynamics of the pump. If the pump pulse has the

zero area, according to the area theorem, its output spectrum has a form of a doublet, whereas for stronger pulses with the areas greater than π , the resonant spectral component (which is equal to the area) takes a nonzero value.

The single-maximum amplification that is obtained from the numerical simulations can be greater than the one observed in the experiments. The discrepancy can be explained by the fact, that this type of amplification appears very close to the resonance frequency, since the spectral width of a smooth soliton is much narrower than that of the broadband polychromatic part (cf. Fig. 12). So, the amplification maximum can be sufficiently reduced by the Doppler broadening of the spectral line, which was not taken into account in the theoretical model presented. On the other hand, the width of the doublet amplification, which appears due to the fast oscillations, can take a value greater than the Doppler linewidth.

C. Strong probe beam and conical emission

Our numerical model describes the interaction of two intersected plane waves. Therefore it does not account for some transverse effects, such as self-focusing of a beam and conical emission. Besides that, since the probe field was treated only in the first order, the model does not describe nonlinear effects in the probe beam.

In the experiment, increase in the probe beam power leads to some asymmetry in the transmission spectrum. In this case, even without the pump beam, the probe beam intensity is sufficient to induce nonlinear effects, which was stressed in Sec. III A. As the pulse duration is shorter than the homogeneous relaxation times, self-induced transparency can dramatically modify the absorption spectrum. It has been shown numerically [31, 32] and proved experimentally [23] that presence of a nonzero detuning δ_0 such that $\gamma_D < \delta_0 < \gamma_{\text{probe}}/2$ results in the appearance of a dispersionlike feature centered at the transition frequency. The spectral components with detunings of the same sign as δ_0 are amplified, and those with opposite sign are attenuated. We suppose that a transmission spectrum plotted in Fig. 5 (curve B) is related to that effect. In our experiment with pulsed discharge, the evolution of the dispersionlike feature under the increase in the metastable atom density, which was described in Sec. III A (measurements were carried out in the presence of the pump beam, its effect is discussed below) is in agreement with numerical results of Ref. [32]. More complicated spectral structure, obtained in Refs. [23, 32] under great optical densities, was unresolved by our apparatus.

Applying a strong pump causes the probe-beam amplification and increases the nonlinear features in its spectrum. It leads to the increase in the probe intensity integrated over the whole spectrum and increases the asymmetry of the transmission spectrum. This effect is clearly seen in Fig. 5.

With a single probe beam, we observed dispersionlike

spectra of both “left” and “right” orientations, in agreement with Refs. [31, 32]. In the presence of the pump beam, a structure with amplification at the blue wing certainly prevails over the opposite one. This fact may be understood, taking into account the effect of resonant self-focusing of the pump beam, which is well pronounced under these experimental conditions. The problem of resonant and near resonant self-focusing and its influence on the propagation of SIT pulses was discussed mostly for relatively narrowband pulses ($\gamma_{\text{pulse}} \approx \gamma_D$). It has been shown numerically [33] and experimentally [34] that during propagation in an extended medium, resonant and slightly blue-detuned SIT pulses become self-focused, while red-detuned pulses experience self-defocusing. This effect strongly modifies transverse profile of the pump beam as well as the profile of the probe, when its intensity becomes sufficiently high. Self-focusing leads to an increase in the axial intensity of the blue components of the probe that increases the effective detuning δ_0 of the central, the most intense part of the beam, and results in more pronounced asymmetry of the transmission spectrum. The interplay between parametric amplification, self- and pump-induced focusing of the probe beam, and propagation effects creates very complex picture, which may be quantitatively described only by numerical modeling.

Conical emission observed in the present experiment appeared under the conditions that are significantly different from other CE experiments. We obtain CE under the metastable atom density of about 10^{13} cm^{-3} and the pump detunings Δ_0 (see Fig. 10) comparable to the Doppler width of the transition, whereas “normal” CE is observed under much greater detunings and mostly under higher medium densities. Besides that, CE observed in the present work is insensitive to the sign of the pump detuning Δ_0 , whereas “normal” CE appears under blue-detuned pump only. The model of Cherenkov-type emission from steady-state self-trapped filaments [18], as well as the steady-state four-wave mixing model [19], seem to be unsuitable under conditions of our experiment. As a nonstationary coherent phenomenon, CE was considered in Refs. [35, 36, 37]. In these works dealing with transform limited pulses, CE was obtained under the breaking up of a laser pulse, which at least qualitatively may also correspond to our results. The shape of CE spectrum presented here is similar to the amplified probe-beam spectrum observed under the same conditions. We suppose that the mechanisms of these two phenomena are closely related.

V. CONCLUSION

The detailed investigation of changes in the spectrum of a polychromatic probe field, which arise during its propagation in a dense resonant medium, is presented. The spectral width of the radiation considered greatly exceeds both the homogeneous and inhomogeneous widths

of the spectral line. In the simplest case of a single-beam propagation, the dispersionlike asymmetry of the transmission spectrum was observed, which was treated as a feature of near resonant self-induced transparency in the so-called sharp line limit. When two laser beams are intersected in a medium, we observed dramatic changes in the probe-beam spectrum: pump-induced amplification and attenuation. The shape of the transmission spectrum depends on the pump and probe intensities, pump detuning, and atomic density. Under relatively weak pumping and high medium density, when the condition of strong coupling between field and resonant matter is fulfilled, the probe amplification spectrum has a form of spectral doublet. Stronger pumping leads to the appearance of a single peak of the probe beam amplification at the transition frequency, manifesting that strong-field effects prevail over effects in a strongly coupled field-matter system. The greater probe intensity results in an asymmetrical transmission spectrum with amplification at the blue wing of the absorption line and attenuation at the red one. Under high medium density, a broad band of amplification appears. Since, in the situation considered, the field of medium reaction plays an important role and forms a significant part of the coherent collective response of a dense medium, the amplification spectra observed differ from the well-known Mollow-Boyd spectra, which

are determined by characteristics of the strong external field. The theoretical model presented is based on the numerical solution of the Maxwell-Bloch equations for two plane waves propagating in a dense extended medium. It is shown that the characteristic features of the probe amplification could be determined by the coherent non-stationary dynamics of the pump field, particularly by the formation of solitons and optical ringing. In some cases, the pump-beam transverse profile also should be taken into account. Under the certain conditions, the periphery area of the pump beam becomes amplified and produces a conical emission. Some parameters of CE obtained in the present work differ from usually observed CE. It should be pointed out that amplified probe-beam spectra reproduce the most characteristic features of generation spectrum of a broadband laser with an intracavity absorbing cell, when the self-frequency-locking effect, i.e., spectrum condensation, takes place [8, 9].

Acknowledgments

The work was partially supported by the INTAS, Project No. 99-1366.

-
- [1] V. V. Zheleznyakov, V. V. Kocharovsky, and V. V. Kocharovsky, *Usp. Fiz. Nauk* **159**, 193 (1989) [*Sov. Phys. Usp.* **32**, 835 (1989)].
- [2] Y. Kaluzny, P. Goy, M. Gross, J. P. Raimond, and S. Haroche, *Phys. Rev. Lett.* **51**, 1175 (1983).
- [3] Y. Zhu, D. J. Gauthier, S. E. Morin, Q. Wu, H. J. Carmichael, and T. W. Mossberg, *Phys. Rev. Lett.* **64**, 2499 (1990).
- [4] S. Prasad and R. J. Glauber, *Phys. Rev. A* **61**, 063814 (2000).
- [5] A. Huynh, J. Tignon, P. Roussignol, C. Delalande, R. Andre, R. Romestain, and D. L. S. Dang, *Phys. Rev. B* **66**, 113301 (2002).
- [6] G. Messin, J. P. Karr, A. Baas, G. Khitrova, R. Houdre, R. P. Stanley, U. Oesterle, and E. Giacobino, *Phys. Rev. Lett.* **87**, 127403 (2001).
- [7] P. G. Savvidis, J. J. Baumberg, R. M. Stevenson, M. S. Skolnick, D. M. Whittaker, and J. S. Roberts, *Phys. Rev. Lett.* **84**, 1547 (2000).
- [8] Y. H. Meyer, *Opt. Commun.* **30**, 75 (1979).
- [9] V. V. Vasil'ev, V. S. Egorov, A. N. Fedorov, and I. A. Chekhonin, *Opt. Spectrosc.* **76**, 146 (1994) [*Opt. Spectrosc.* **76**, 134 (1994)].
- [10] S. G. Rautian and I. I. Sobel'man, *Zh. Eksp. Teor. Fiz.* **41**, 456 (1961) [*Sov. Phys. JETP* **14**, 328 (1962)].
- [11] B. R. Mollow, *Phys. Rev. A* **5**, 2217 (1972).
- [12] R. W. Boyd, M. G. Raymer, P. Narum, and D. J. Harter, *Phys. Rev. A* **24**, 411 (1981).
- [13] D. J. Harter, P. Narum, M. G. Raymer, and R. W. Boyd, *Phys. Rev. Lett.* **46**, 1192 (1981).
- [14] W. Chalupczak, W. Gawlik, and J. Zachorowski, *Phys. Rev. A* **49**, 4895 (1994).
- [15] F. Y. Wu, S. Ezekiel, M. Ducloy, and B. R. Mollow, *Phys. Rev. Lett.* **38**, 1077 (1977).
- [16] P. Weisman, A. D. Wilson-Gordon, and H. Friedmann, *Phys. Rev. A* **61**, 053816 (2000).
- [17] D. Grischkowsky, *Phys. Rev. Lett.* **24**, 866 (1970).
- [18] B. D. Paul, J. Cooper, A. Gallagher, and M. G. Raymer, *Phys. Rev. A* **66**, 063816 (2002).
- [19] F. Valley, G. Khitrova, H. M. Gibbs, J. W. Grantham, and X. Jiainin, *Phys. Rev. Lett.* **64**, 2362 (1990).
- [20] Y. H. Meyer, *Opt. Commun.* **34**, 439 (1980).
- [21] R. C. Hart, L. You, A. Gallagher, and J. Cooper, *Opt. Commun.* **111**, 331 (1994).
- [22] Y. Ben-Aryeh, *Phys. Rev. A* **56**, 854 (1997).
- [23] J. K. Ranka, R. W. Schirmer, and A. L. Gaeta, *Phys. Rev. A* **57**, R36 (1998).
- [24] N. Schupper, H. Friedmann, M. Matusovsky, M. Rosenbluh, and A. D. Wilson-Gordon, *J. Opt. Soc. Am. B* **16**, 1127 (1999).
- [25] S. N. Bagaev, V. S. Egorov, I. B. Mekhov, P. V. Moroshkin, and I. A. Chekhonin, *Opt. Spectrosc.* **93**, 1033 (2002) [*Opt. Spectrosc.* **93**, 955 (2002)].
- [26] S. N. Bagayev, V. S. Egorov, I. B. Mekhov, P. V. Moroshkin, A. N. Fedorov, I. A. Chekhonin, E. M. Davliatchine, and E. Kindel, *Proc. SPIE* **4748**, 45 (2002).
- [27] S. N. Bagaev, V. S. Egorov, I. B. Mekhov, P. V. Moroshkin, and I. A. Chekhonin, *Opt. Spectrosc.* **94**, 99 (2003) [*Opt. Spectrosc.* **94**, 92 (2003)].
- [28] L. Allen and J. H. Eberly, *Optical Resonance and Two-level Atoms* (Wiley, New York, 1975).
- [29] G. L. Lamb, *Rev. Mod. Phys.* **43**, 99 (1971).

- [30] M. D. Crisp, *Phys. Rev. A* **1**, 1604 (1970).
- [31] J. C. Diels and E. L. Hahn, *Phys. Rev. A* **8**, 1084 (1973).
- [32] W. Miklaszewski, *J. Opt. Soc. Am. B* **12**, 1909 (1995).
- [33] F. P. Mattar and M. C. Newstein, *IEEE J. Quantum Electron.* **13**, 507 (1977).
- [34] H. M. Gibbs, B. Boelger, F. P. Mattar, M. C. Newstein, G. Forster, and P. E. Toschek, *Phys. Rev. Lett.* **37**, 1743 (1977).
- [35] W. Gawlik, R. Shuker, and A. Gallagher, *Phys. Rev. A* **64**, 021801(R) (2001).
- [36] M. E. Crenshaw, and C. D. Cantrell, *Phys. Rev. A* **39**, 126 (1989).
- [37] A. N. Starostin, A. A. Panteleev, V. I. Lebedev, S. V. Rotin, A. G. Leonov, and D. I. Chekhov, *Zh. Eksp. Teor. Fiz.* **108**, 1203 (1995) [*Sov. Phys. JETP* **81**, 660 (1995)].
- [38] V. S. Egorov, V. N. Lebedev, I. B. Mekhov, P. V. Moroshkin, I. A. Chekhonin, and S. N. Bagayev, *quant-ph/0308155*.

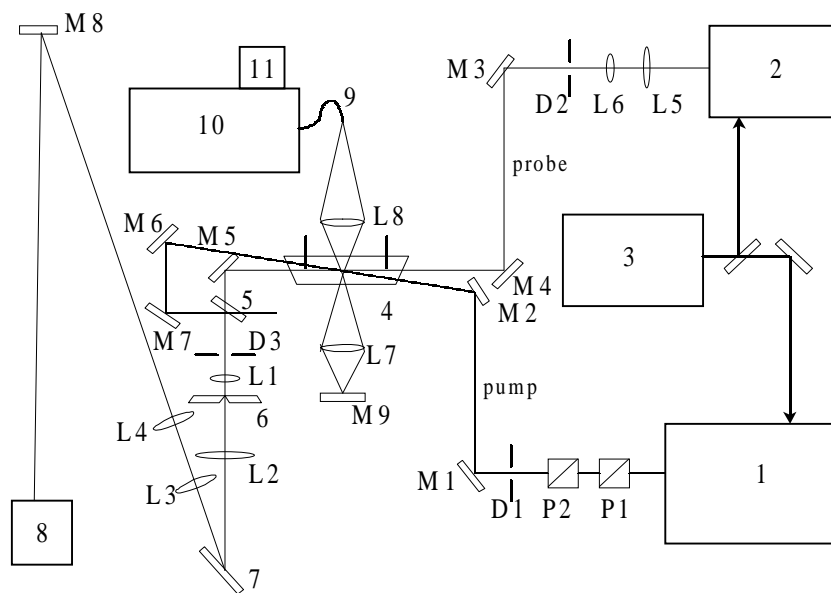


FIG. 1: Scheme of the experimental setup: 1, 2, dye lasers; 3, Nd:YAG laser; 4, discharge tube; 5, beam splitter; 6, slit; 7, diffraction grating (2400 grooves/mm); 8, optical multichannel analyzer (OMA); 9, fiber; 10, spectrograph; 11, OMA; M1 - M9, mirrors; L1 - L8, lenses; D1 - D3, diaphragms; P1, P2, polarizers.

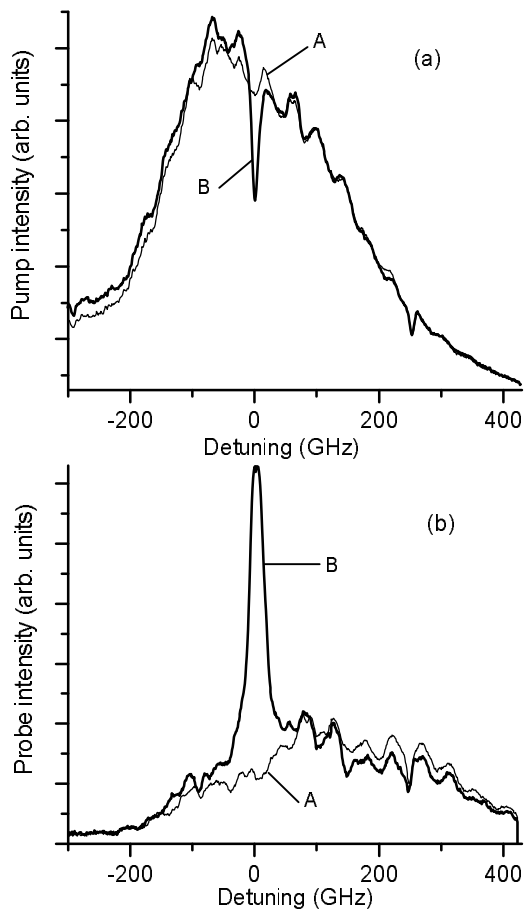


FIG. 2: Dye-laser spectra: (a) the pump beam in a broadband mode; (b) the probe beam; dc discharge, $P = 0.9$ Torr, $I = 20$ mA, $\lambda = 640.2$ nm, $n_0 = 10^{12}$ cm $^{-3}$, $\alpha_0 L = 20$; A, original dye laser spectrum; B, the spectrum after interaction with the medium.

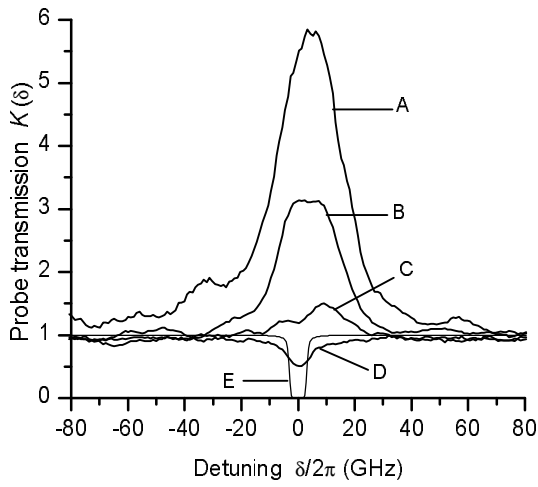


FIG. 3: Probe-beam transmission spectra at different pump powers; dc discharge, $P = 1.2$ Torr, $I = 10$ mA, $\lambda = 640.2$ nm, $n_0 = 10^{12}$ cm $^{-3}$, $\alpha_0 L = 20$, broadband pump; A, $W = 76$ μ J; B, $W = 60$ μ J; C, $W = 30$ μ J; D, $W = 0$; E, calculated classical absorption-line contour.

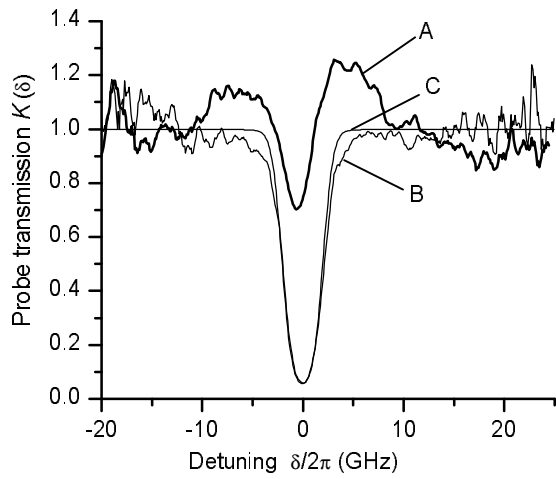


FIG. 4: Probe-beam transmission spectra recorded with a Fabry-Perot interferometer; dc discharge, $P = 1$ Torr, $I = 50$ mA, $\lambda = 588.2$ nm, $n_0 = 6 \times 10^{11}$ cm $^{-3}$, $\alpha_0 L = 2$, $W \approx 1$ μ J; A, the pump beam on; B, the pump beam off; C, calculated classical absorption-line contour.

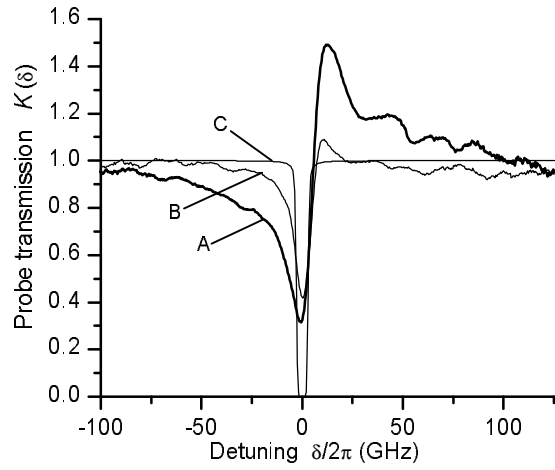


FIG. 5: Probe-beam transmission spectra in the case of strong probe beam; dc discharge, $P = 1.2$ Torr, $I = 10$ mA, $\lambda = 640.2$ nm, $n_0 = 10^{12}$ cm $^{-3}$, $\alpha_0 L = 20$, $W = 26$ μ J, broadband pump; A, the pump beam on; B, the pump beam off; C, calculated classical absorption-line contour.

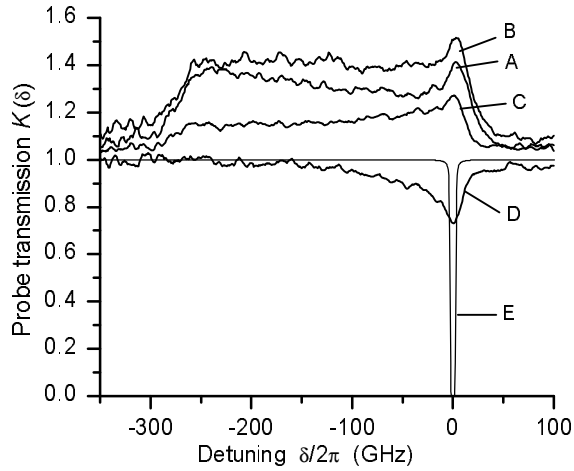


FIG. 6: Probe-beam transmission spectra at different time delays; pulsed discharge afterglow, $P = 9.0$ Torr, $I = 4.0$ A, $t_p = 100$ μ s, $\lambda = 640.2$ nm, $n_0 \approx 10^{13}$ cm $^{-3}$, $\alpha_0 L \approx 200$, $W = 76$ μ J, broadband pump; A, $\tau_d = 30$ μ s; B, $\tau_d = 80$ μ s; C, $\tau_d = 180$ μ s; D, $\tau_d = 30$ μ s with pump beam off; E, calculated classical absorption-line contour.

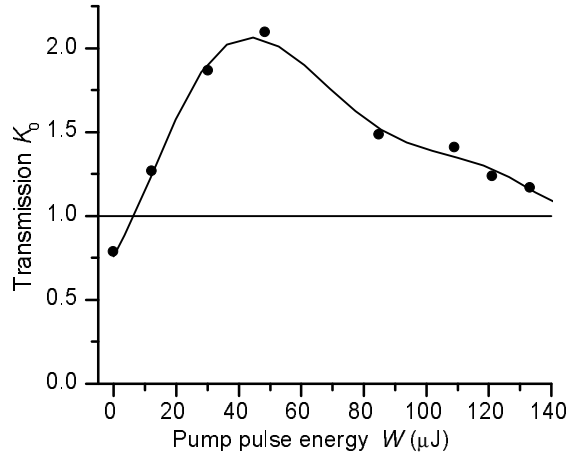


FIG. 7: Dependence of the transmission at the resonance frequency K_0 on the pump pulse energy W ; dc discharge, $P = 1.2$ Torr, $I = 10$ mA, $\lambda = 640.2$ nm, $n_0 = 10^{12}$ cm $^{-3}$, $\alpha_0 L = 20$, broadband pump, transmission spectrum belongs to the first type.

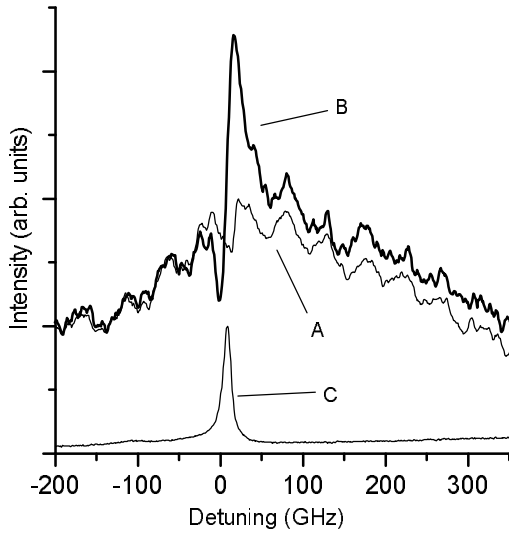


FIG. 8: Experiment with narrowband pump; dye-laser spectra; pulsed discharge afterglow, $P = 14$ Torr, $I = 4.5$ A, $t_p = 100$ μs , $\tau_d = 50$ μs , $\lambda = 640.2$ nm, $n_0 \approx 10^{13}$ cm $^{-3}$, $\alpha_0 L \approx 200$, $W = 20$ μJ ; A, original probe beam; B, the probe beam after interaction with the medium; C, the pump beam in a “narrowband” mode; spectral intensities of probe and pump fields are presented in different arbitrary units.

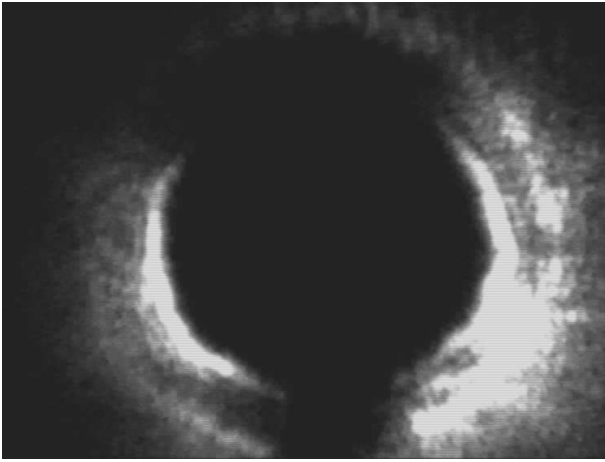


FIG. 9: Pump-beam transverse structure at the output of the discharge tube; pulsed discharge afterglow, $P = 14$ Torr, $I = 4.5$ A, $t_p = 80 \mu\text{s}$, $\tau_d = 40 \mu\text{s}$, $\lambda = 640.2$ nm, $W = 10 \mu\text{J}$, narrowband pump, $\Delta_0 = 0$; central part of the beam is blocked.

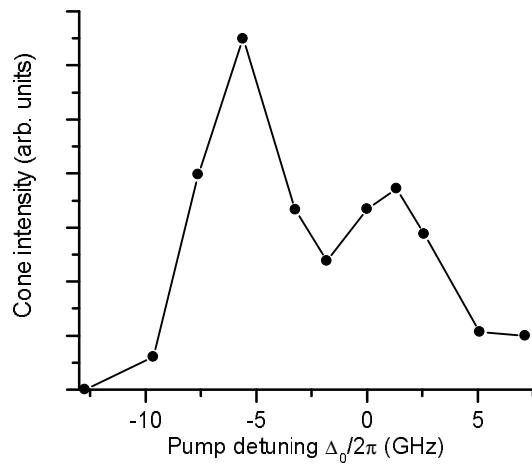


FIG. 10: Cone intensity dependence on the pump detuning Δ_0 ; pulsed discharge afterglow, $P = 14$ Torr, $I = 4.5$ A, $t_p = 80 \mu\text{s}$, $\tau_d = 20 \mu\text{s}$, $\lambda = 640.2$ nm, $W = 10 \mu\text{J}$, narrowband pump.

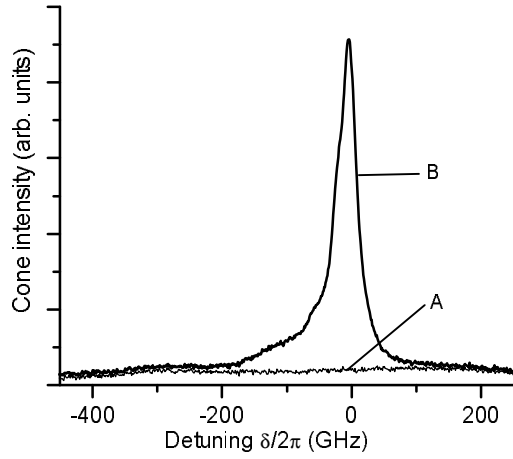


FIG. 11: Conical emission spectrum; pulsed discharge after-glow, $P = 9$ Torr, $I = 4.0$ A, $t_p = 100 \mu\text{s}$, $\tau_d = 16 \mu\text{s}$, $\lambda = 640.2$ nm, $W = 53 \mu\text{J}$, broadband pump; A, discharge off; B, discharge on.

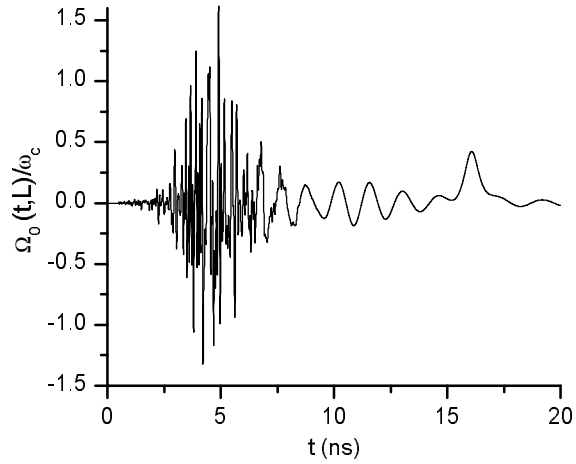


FIG. 12: Temporal behavior of a polychromatic pulse after propagation in an extended resonant medium; numerical modeling, $\omega_c/2\pi = 2.6$ GHz, $L = 15$ cm.

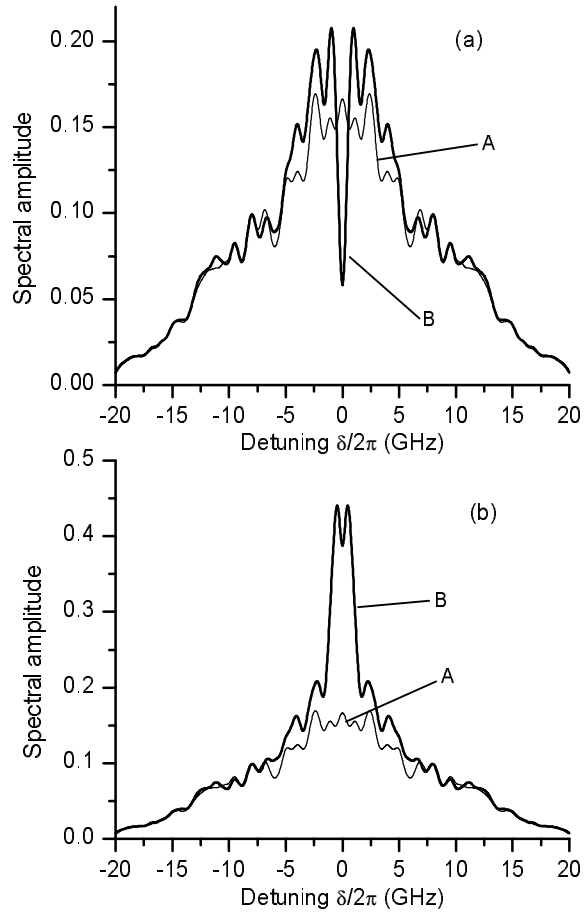


FIG. 13: Calculated spectra of the probe field at the input (curves A) and output (curves B) of a medium; (a) doublet amplification, (b) amplification with resonant maximum; $\omega_c/2\pi = 2.6$ GHz, $L = 15$ cm.